Spinning and Characterizations of Polypropylene/ Alkylphosphonic Acid Treated Montmorillonite Nanocomposite Fiber

Sarit Thanomchat,[1] Sarintorn Limpanart,[2] Kawee Srikulkit[1,3]

[1]*Department of Materials Science, Faculty of Science, Chulalongkorn University, Bangkok 10330, Thailand*
[2]*Metallurgy and Materials Science Research Institute, Chulalongkorn University, Bangkok 10330, Thailand*
[3]*National Center of Excellence for Petroleum, Petrochemicals and Advanced Materials, Bangkok 10330, Thailand*

Received 13 September 2009; accepted 25 December 2009
DOI 10.1002/app.32016
Published online 5 April 2010 in Wiley InterScience (www.interscience.wiley.com).

ABSTRACT: Fine and well-dispersed clay was prepared via the *in situ* conversion of the dodecylamine intercalant inside the clay gallery to dodecylamino dimethylene diphosphonic acid (DDD), using a Mannich reaction, so as to create a repulsive force that delaminated the clay platelets. The clay structure and morphology were characterized by X-ray diffraction (XRD), Scanning electron microscopy (SEM), and Transmission electron microscopy (TEM) analysis, which revealed changes in the multilayer stacks. XRD analysis showed that the interlayer spacing was largely expanded by the presence of DDD. SEM and TEM images revealed that DDD containing clay (PMMT), but not that without DDD, exhibited transparency, indicating the extremely fine and well-dispersed clay. Polypropylene/PMMT nanocomposites containing 2, 4, 6, 8, and 10 wt % PMMT were prepared by melt extrusion. The obtained compounds were each spun into a monofilament fiber using a small scale spinning machine and then characterized by XRD, Differential scanning calorimetry (DSC), and Thermogravimetric analysis (TGA), plus the sonic modulus was evaluated. The XRD results revealed an increase in the β crystallinity peak in fibers loaded with 2–10 wt % PMMT, indicating that PMMT particles were capable of acting as a β-form nucleating agent. However, only minimal changes in the thermal behavior (T_c) were observed due to the tested samples containing insufficient PMMT content. The mechanical properties, in terms of the tensile strength and sonic modulus value (E), of the polypropylene nanocomposite fibers were higher than those of virgin PP fibers, presumably due to the reinforcement effect of the filled PMMT nanoparticles. © 2010 Wiley Periodicals, Inc. J Appl Polym Sci 117: 1969–1977, 2010

Key words: modification of *in situ* dodecylamine intercalant; PP/alkylphosphonic treated nanocomposite fiber; nucleating agent; mechanical properties

INTRODUCTION

Montmorillonite clay is composed of stacks of individual platelets held together by ionic forces. Due to the characteristic layered structure, this type of clay is used in several applications, such as adsorption, ion exchanges, catalysis, and nanocomposites. Polymer–clay nanocomposites have attracted a great deal of attention because they offer enhanced mechanical and thermal properties when compared to conventional composites. Specially, these nanocomposites containing nanosized particles at a much lower loading ratio than conventional fillers exhibit an increased tensile strength, modulus, and heat distortion resistance.[1,2] However, the direct addition of the nanoparticles into the polymer has typically failed to deliver the expected improvements in the above properties due to its incompatibility and lack of dispersibility. Therefore, it is important that, to achieve these improved mechanical and thermal properties, the state of the delaminated structure (nanoscale) with a good dispersion in the polymer matrix is required.[3] Montmorillonite can be delaminated by stirring in a suitable solvent but it restacks to the original form upon solvent evaporation.[4] Typically, the clay is organically modified with a bulky organic cation to make it compatible with a selected polymer,[5–9] and then blended with that polymer via *in situ* polymerization or melt compounding, resulting in a polymer/clay nanocomposite with enhanced properties. The structure of the organoclay usually exhibits a certain degree of interspacing expansion, which is further expanded by penetration of the polymer molecule, resulting in exfoliated platelets that are responsible for the enhanced thermal and mechanical properties of the polymer nanocomposites. Therefore, the preparation of the intercalated clay is crucial to facilitate the even dispersion of the nanoscale sized clay particles, particularly when being incorporating into synthetic fibers during the

Correspondence to: K. Srikulkit (kawee@sc.chula.ac.th).
Contract grant sponsors: National Science and Technology Development Agency, Thailand; Thailand Research Fund.

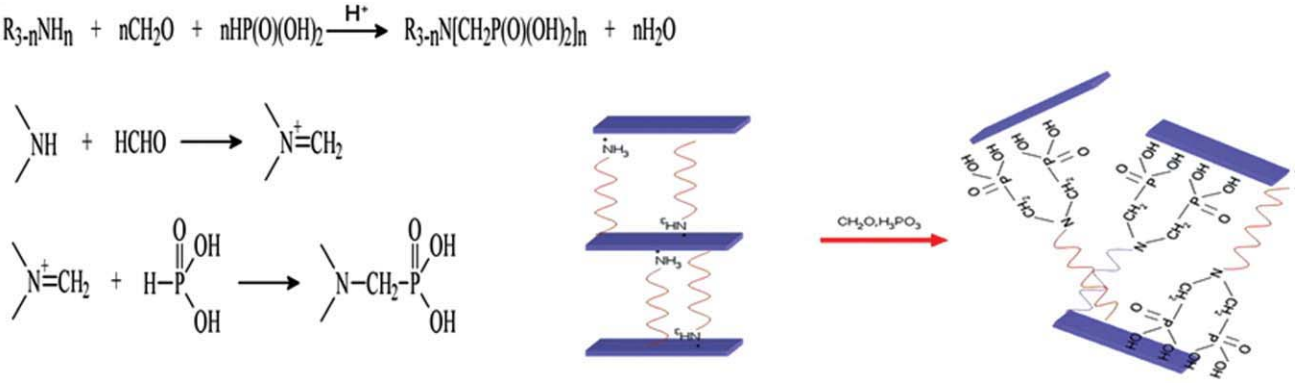

Scheme 1 *In situ* conversion of dodecylamine to dodecylamino dimethylene diphosphonic acid by the Mannich reaction. [Color figure can be viewed in the online issue, which is available at www.interscience.wiley.com.]

melt-spinning process due to the high speed spinning rate. Polypropylene is one of the synthetic fibers that are commonly found in many end-use products due to its advantageous properties, such as light weight, resistance to moisture and chemicals, low cost, sufficiency strength, and ease in processing. Furthermore, the fiber's properties can be enhanced by melt mixing with particulates and fibrous materials as well as by melt blending with other polymers.[10–14] Nanometer scale particles as fillers have attracted interest as a means for enhancing the properties of polymeric materials. Particularly, carbon nanotube (CNT)[15,16] and montmorillonite (MMT)[17,18] have taken a lead as nanofillers for plastics as well as fibers. In this study, polypropylene/clay nanocomposite fibers were prepared. Montmorillonite clay was modified to achieve an organoclay with larger interspacing, aimed at forming an exfoliated clay powder, which is expected to readily disperse in the polymer matrix. Then, a PP/organoclay nanocomposite resin was obtained using a twin-screw extruder and spun into filaments using a small scale spinning machine (Bradford University Research). Finally, characterization of the filaments, including by XRD, TEM, and SEM analysis, were carried out and are discussed.

EXPERIMENTAL

Materials

Na-bentonite with a cation exchange capacity (CEC) of 72 meq/100 g clay was purchased from Southern Clay Products; Dodecylamine was purchased from Fluka (Switzerland). Phosphorus acid and paraformaldehyde were purchased from Aldrich (Germany). HCl (analytical grade, 37 wt %) was bought from Schlarlua. Moplen® (isotactic polypropylene) chips, with a melt flow index of 25.8 g/10 min at 190°C, were purchased from HMC Polymers Co., (Thailand) and were ground into powder by THL Industry Co., (Thailand). Licocene® PP 6120 was kindly provided by Clariant Ltd. Irganox® 1010, a heat stabilizer, was purchased from Ciba Specialty Chemicals (Thailand).

Intercalation of montmorillonite with dodecylamine and *in situ* conversion into dodecylamino dimethylene diphosphonic acid by the Mannich reaction

A typical procedure was as follows:[19] A 50 g portion of Na-montmorillonite was suspended in 500 mL of deionized water in a 1000-mL three-necked flask and 6.24 mL of dodecylamine (0.27 mol; equal to 7.5 times of the cation exchange capacity (CEC)) was added to the suspension followed by the slow addition of 89 mL of 37 wt % HCl (four times higher molar concentration than that of the dodecylamine amino groups). Dodecylamine was slowly protonated and solubilized. The mixture was gradually heated to 80°C and mechanically stirred for 2 h to allow the maximum cation exchange reaction. A sample of the organoclay was taken for subsequent characterization, and to the rest was added crystalline phosphorous acid (0.54 mol, two times higher than the dodecylamine concentration). The three-necked flask was then fitted with a thermometer, condenser, and dropping funnel. Over the course of ca. 1 h, 16.22 g of formaldehyde (2 : 1 mole ratio of formaldehyde to dodecylamine) was added drop by drop, and the reaction maintained at 80°C for an additional hour. It was anticipated that intercalated dodecyl ammonium as well as free dodecyl ammonium would be completely converted into dodecylamino dimethylene diphosphonic acid (DDD). Then, the treated clay (DDD-montmorillonite or PMMT) was filtered-off and dried in an oven at 60°C for 24 h. Due to the loss of formaldehyde from side reactions, formaldehyde to dodecylamine mole ratios were varied from 2 : 1, 3 : 1, 4 : 1, 5 : 1, and 6 : 1. A schematic diagram of the Mannich reaction is shown in Scheme 1.

TABLE I
Composition of PP/PMMT Nanocomposite Formulation

Composition	Batch No./wt (g)					
	1	2	3	4	5	6
PMMT	0	6 (2 wt %)	12 (4 wt %)	18 (6 wt %)	24 (8 wt %)	36 (10 wt %)
iPP Powder	239.25	233.25	227.25	221.25	215.25	209.25
PP wax	60	60	60	60	60	60
Irganox (Heat Stabilizer)	0.75	0.75	0.75	0.75	0.75	0.75
Total	300.00	300.00	300.00	300.00	300.00	300.00

Clay characterizations

FTIR spectroscopy, taken on KBr pellet samples, was recorded on a Nicolet Fourier transform spectrophotometer (Nicolet Impact 400D). X-ray diffraction was performed using a PW 3710 Philips diffractometer with CuK_α radiation ($\lambda = 0.1542$ nm) operated at 40 kV and 30 mA. The morphology of the clay sample powder was observed by scanning electron microscopy using a JEOL scanning electron microscope, JSM-5410LV. TEM micrographs were taken from a JEM-2100 TEM, Jeol, Japan.

Fiber spinning

Before spinning, the PMMT/PP composite compound was prepared by melt blending via a twin-screw extruder as follows: Weighed PMMT and PP wax (two times the amount of wax) were premelt mixed using a hot plate. Then, the PP wax/PMMT mixture, PP powder and heat stabilizer were melt mixed using the twin-screw extruder. The as-extruded resin so obtained was fed into the small-scale fiber spinning machine to produce filament fiber. A series of filament fibers, containing 0, 2.0, 4.0, 6.0, 8.0, and 10 wt % PMMT, were spun, with the detailed compositions outlined in Table I. For fiber spinning; the as-extruded resin was fed into the spinning machine's extruder where the barrel temperature was at 210°C. Take-up roller 1 and 2 were set at speeds of 3 m and 60 m/min, respectively. It should be pointed out that in the case of the 8 wt % PMMT loaded fiber, a slightly lower take-up speed of roller 2 was employed. For 10 wt % PMMT loaded fiber, a take-up speed of only 3 m/min was applied due to the problem of filament breakage at higher speeds.

Fiber characterizations

The fiber morphology was examined by optical microscopy using an Olympus BX60 with moticam 2300. XRD patterns of the fiber samples were achieved using a Bruker - D8 Advance model with CuKα radiation at a wave length of 1.5 Å. The diffraction spectrogram was recorded in the 2θ (2 theta) range from 10 to 50°. Thermogravimetric analysis (TGA) analysis was performed with a TGA/SDTA851[e] Mettler Toledo thermal analyzer, with a heating rate of 10°C/min from 50 to 600°C under nitrogen gas at a constant flow rate of 20 mL/min. Differential scanning calorimetry (DSC 200 F3 from NETZSCH) was performed to obtain the crystallization temperature. Melt flow index (MFI) was carried out using Kayaness according to the ASTM 1230 method. Sonic modulus analysis, with a Dynamic Modulus Tester PPM-5R, Lawson-Hemphill Company, was employed to determine the molecular orientation along the fiber axis.

RESULTS AND DISCUSSION

Clay characterizations

The FTIR spectra of dodecylamine intercalated clay and DDD treated clay are shown in Figure 1. Dodecylamine intercalated clay [Fig. 1(a)] exhibited a distinctive absorption band at ~2921 cm^{-1}, which corresponds to stretching of the dodecylamine C—H bond. In addition, the C—N band appears at 1081 cm^{-1}. However, the absorption band associated with the amine ($-NH_3^+$) group, typically found in the region of 1450–1500 cm^{-1} was not observed,

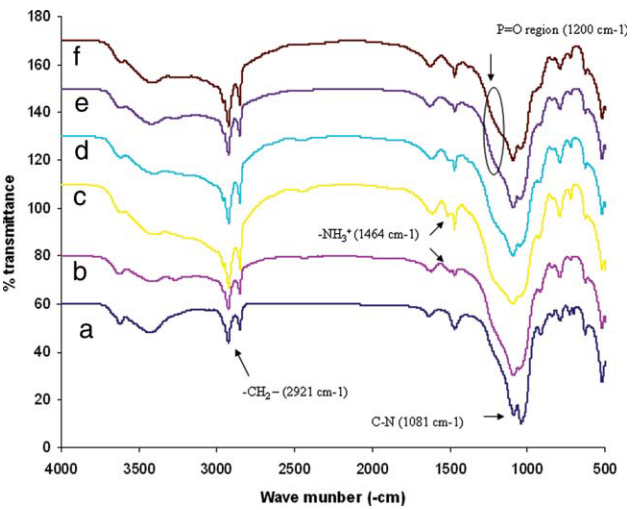

Figure 1 FTIR spectra of dodecylamine-clay and dodecylamino dimethylene diphosphonic acid (DDD)-clays. [Color figure can be viewed in the online issue, which is available at www.interscience.wiley.com.]

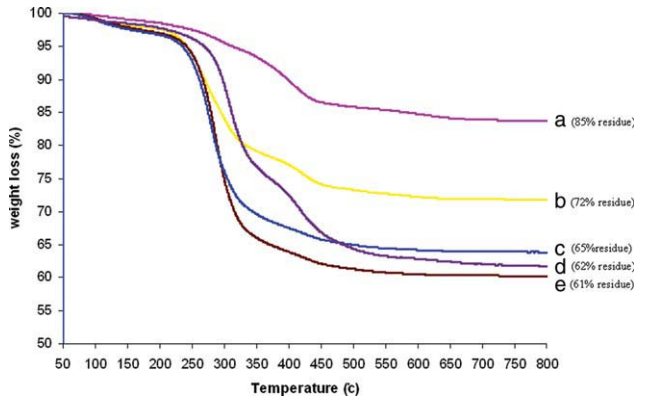

Figure 2 TGA thermograms of dodecylamine-clay and dodecylamino dimethylene diphosphonic acid (DDD)-clays. [Color figure can be viewed in the online issue, which is available at www.interscience.wiley.com.]

probably due to the suppressive effect derived from the ionic interaction between $-NH_3^+$ groups and the negative charge on the clay surface. Changes in the FTIR spectra [Fig. 1(b–f)] were observed for DDD-clays as a result of the conversion of the $-NH_3^+$ group to diphosphonic acid groups by the Mannich reaction (Scheme 1), where the intensity of the C—N—C band produced from the reaction, when compared to an adjacent peak (as a reference), increases as the mole ratio of formaldehyde : dodecylamine increases [Fig. 1(b–f)], confirming the Mannich reaction. In a classical Mannich reaction, the intermediate iminium ion is formed from the reaction of free amine (dodecylamine) and formaldehyde under acidic conditions. Unfortunately, under such conditions, some formaldehyde can be converted to trioxane/polyoxymethylene as a side reaction product.[20] Therefore, in this study, an excess amount of formaldehyde (formaldehyde : dodecylamine ratio >2 : 1) was employed to compensate for the loss of formaldehyde to the side reaction.

The $-NH_3^+$ peak at 1464 cm^{-1} decreases with increasing formaldehyde: dodecylamine molar ratios and finally disappears when the formaldehyde : dodecylamine ratio reaches 6 : 1 [Fig. 1(f)], indicating the completeness of the reaction. It should noted that in case of DDD-clays with an incomplete conversion of dodecylamine, the absorption band of $-NH_3^+$ group can be observed, as the *in situ* dodecylphosphonic acids exhibits a repulsive interaction with the clay surface, rendering the unreacted dodecylammonium ion detached from the clay surface. FTIR spectra further confirm that the absorption bands responsible for the characteristics of dodecylamino dimethylene diphosphonic acid appear clearly at 2900 cm^{-1} (C—H stretching) and the broad 1240–1200 cm^{-1} peak (phosphoryl P=O vibration).

TGA thermograms of DDD-clays are shown in Figure 2. As seen, the residual weight gradually decreases with an increase in the formaldehyde : dodecylamine molar ratios. Namely, a 85, 72, 65, 62, and 61% residue is found for dodecylamine-clay [Fig. 2(a)] and DDD-clays obtained from the formaldehyde : dodecylamine ratios of 2 : 1 (B), 4 : 1 (C), 5 : 1 (D), and 6 : 1 (E), respectively. These reflect that DDD-clay contains a higher DDD content (organic content) as the formaldehyde : dodecylamine ratios increase as a result of the increasing conversion yield. From the formaldehyde : dodecylamine ratio of 5 : 1 to 6 : 1, the increment in the DDD content is insignificant, indicating the optimum yield of the reaction. Therefore, in this study, only DDD-clay produced from the formaldehyde: dodecylamine ratio of 6 : 1 was employed for the preparation of nanocomposite fibers.

X-ray diffraction (XRD) is an effective method for the investigation of the intercalation existence of montmorillonite. The wide angle X-ray diffraction patterns of modified montmorillonites in the region between $2\theta = 3°$ and $2\theta = 25°$ are shown in Figure 3. Typically, the X-ray diffractogram of pristine montmorillonite shows a single peak at $2\theta = 7.13°$, corresponding to the 001 lattice spacing of the silicate layer in montmorillonite. The X-ray diffractogram of dodecylamine treated montmorillonite shows the diffraction peak of the 001 lattice spacing of the silicate layer shifting from $2\theta = 7.13°$ to $2\theta = 5.23°$. According to Bragg's law, the interlayer spacing corresponding to these peaks increases from 12.39 Å ($2\theta = 7.13°$) to 16.848 Å ($2\theta = 5.23°$). Presumably, the cationic exchange reaction between the dodecyl ammonium and Na^+ ion residing in the interspacing layer took place during the interaction step. Subsequent *in situ* conversion of the dodecyl ammonium intercalant ($R—NH_3^+$) into dodecylamino dimethylene diphosphonic acid ($R—N\{CH_2P(O)(OH)_2\}_2$) caused several notable changes in the observed XRD patterns, particularly the intensity of

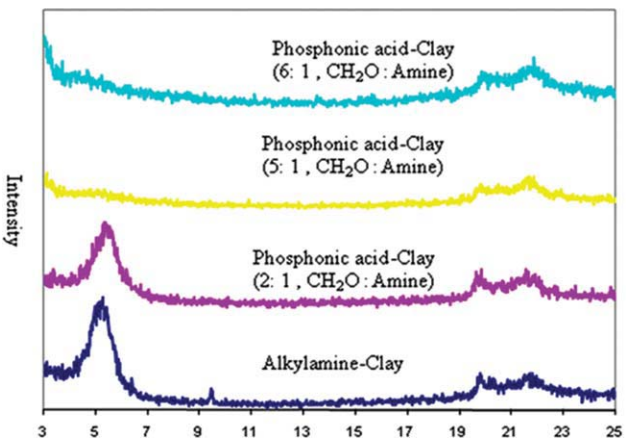

Figure 3 XRD diffractograms of clays. [Color figure can be viewed in the online issue, which is available at www.interscience.wiley.com.]

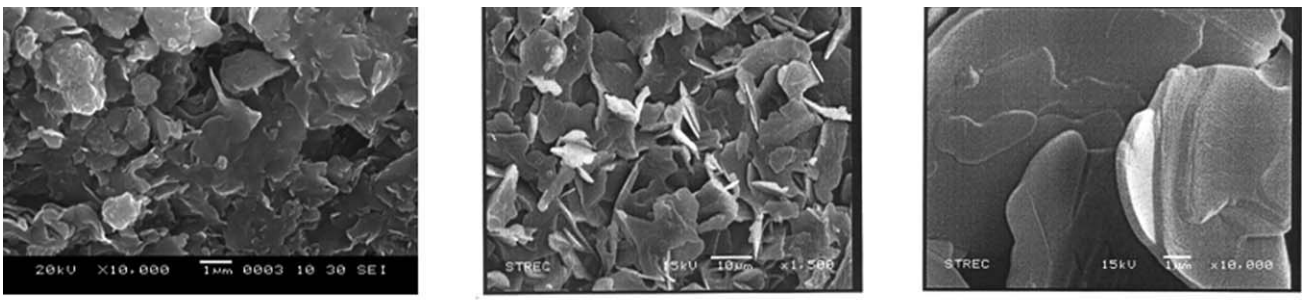

Figure 4 SEM images of (a) alkylamine-clay, (b, c) dodecylamino dimethylene diphosphonic acid-clays.

the peak signal at 5.23°, which is significantly reduced as the percent conversion of dodecylamine to dodecylamino dimethylene diphosphonic acid is increased. The extent of the conversion was adjusted by varying the molar intercalant dodecylamine: formaldehyde ratios from 2 : 1 to 6 : 1. At a low formaldehyde : dodecylamine molar ratio (2 : 1), no difference was observed in the XRD patterns between the organoclay and DDD-clay. At higher ratios (5 : 1 and 6 : 1), the disappearance of the 001 lattice spacing peak from the DDD-montmorillonite was observed, suggesting that the whole population of intercalated montmorillonite reaches a state of total expansion. This phenomenon could be explained by the fact that, because of the Mannich reaction, the ionic bond between the negatively charged clay and dodecyl ammonium cation was diminished and replaced with repulsive interactions instead. As a consequence, the DDD formed inside the montmorillonite gallery plays a key role in expanding the gallery spacing. The characteristic structure of the clay mineral is evident from the existence of the two dimensional reflection in the region of $2\theta = 20$–$22°$.

SEM images of montmorillonite clays revealed that the dodecylamine intercalated clay (organoclay) particles [Fig. 4(a)] were adhered together in an agglomerate form. The organophilic surface derived from the surfactant coverage was probably responsible for causing the particles to stick together during drying. In contrast, the clay containing DDD were clearly visualized as scattered individual particles with a submicron-sized diameter that were separate from one another [Fig. 4(b,c)]. Thus, it remains plausible that during the course of dodecylamine–dodecylamino dimethylene diphosphonic acid conversion, exfoliated platelets underwent restacking with the formation of large platelets. A similar phenomenon of large platelet formation has been observed during the recovery of organoclay from nitrobenzene dispersion.[4] When considering each piece of particle, the platelike structure of individual layers is revealed. In general, the particle thickness is found to be less than ~500 nm. However, it still appears that the clay particle consists of multilayered stacks.

TEM micrographs of the DDD-clay reveal that despite its presence in multilayer stacks, the DDD containing clay exhibits transparency to TEM (Fig. 5), indicating that extremely fine platelet formation was achieved. This transparent TEM image is not seen with either the parent clay or conventional organoclay, which typically comprises of stacks of over 100 layers. Therefore, it is reasonable to assume that the synthesis of DDD inside the clay gallery could separate stacks of clay platelets by creating a powerful enough repulsion force between the diphosphonic acid groups and the negatively charged clay to force apart the platelet stacks (schematically shown in Scheme 1).

Fiber characterizations

Fiber morphology

The fiber morphology, as seen by optical microscopy, of neat PP and PP/PMMT composite filaments

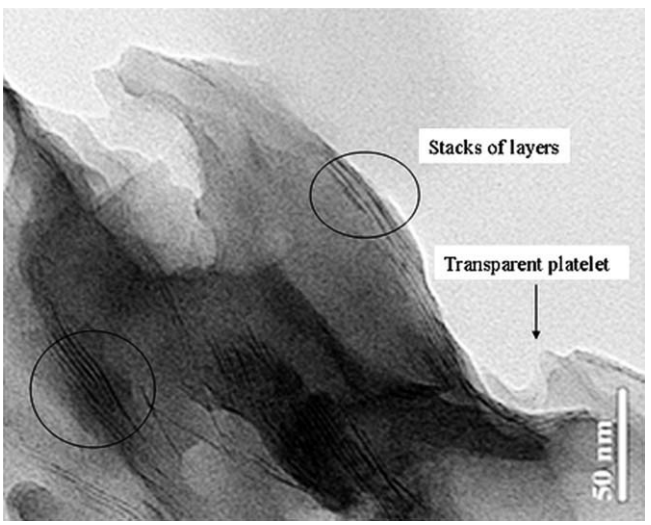

Figure 5 TEM micrographs of dodecylamino dimethylene diphosphonic acid-clay.

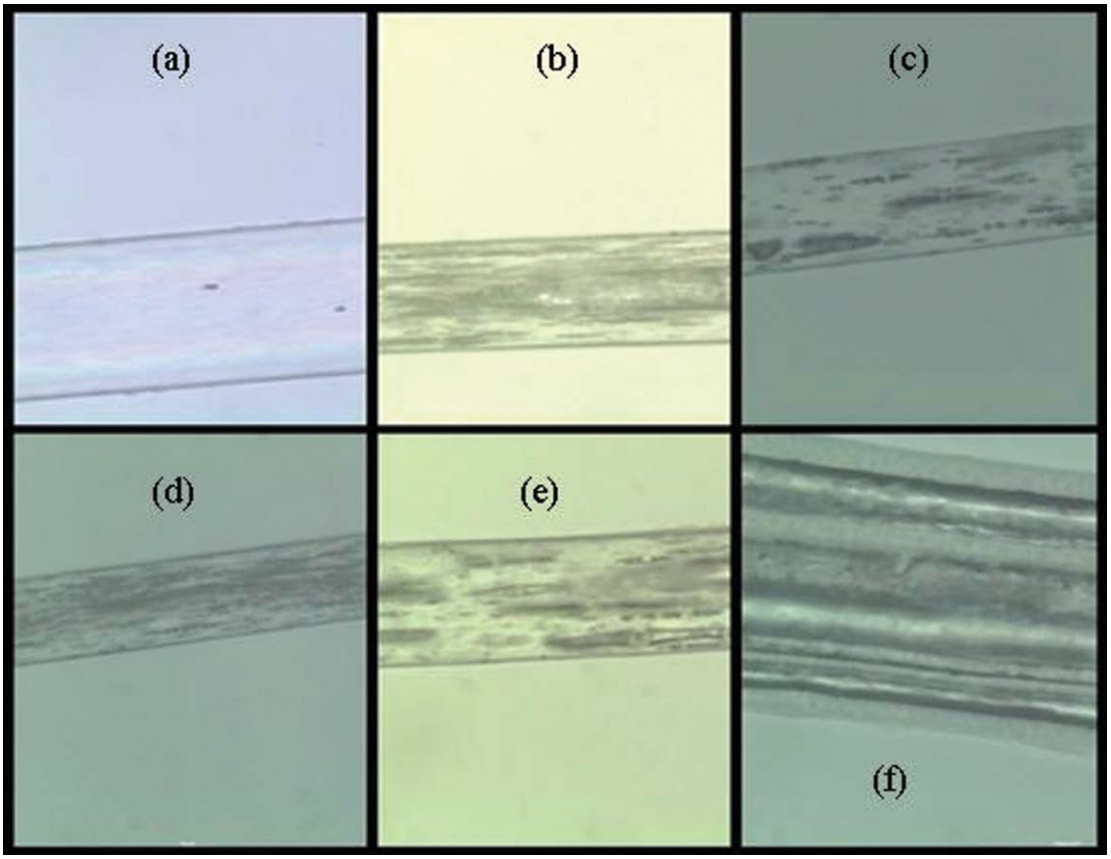

Figure 6 The optical microscopic images of fiber morphology (a = neat fiber, b = 2 wt %, c = 4 wt %, d = 6 wt %, e = 8 wt %, and f = 10 wt % PMMT). [Color figure can be viewed in the online issue, which is available at www.interscience.wiley.com.]

are shown in Figure 6 where, in general, the filaments containing 2–6 wt % PMMT loadings exhibited a smooth surface, but higher PMMT loadings above 6 wt % had a notable rough surface, presumably due to the poorer dispersion of PMMT particles. With respect to the fiber diameter, an increase in PMMT loading from 2 to 4, 6, and 8 wt % leads to a reduction in the average fiber diameter from 84 to 65, 68, and 80 microns, respectively, (compared to 90 microns for the pristine PP fiber). Note that the 10 wt % PMMT/PP fiber was exempted from this analysis as draw take-up was not applied due to filament breakage. In this case, the obtained fiber diameter was measured from the as-spun fiber (199 micron). The reduction in the nanocomposite fiber diameter was associated with the change in its rheological behavior, where the MFI values of nanocomposite compounds containing 0, 2, 4, 6, 8, and 10 wt % PMMT were 47.12, 52.80, 54.27, 60.94, and 64.34 g/10 min, respectively, indicating that an increase in the PMMT loading leads to a steady decrease in the melt viscosity of the nanocomposite. In contrast, previous reports have suggested that the presence of exfoliated clay increases the polymer matrix viscosity due to the interfacial interaction between the nanoscale filler and polymer chain. Regardless, the increased viscosity with increasing PMMT loadings observed in this study fits with the characteristics of internal lubrication, which is a phenomenon of the apparent reduction of polymer melt viscosity caused by an internal lubricant. Examples of internal lubricants are typically polar molecules such as fatty acids, fatty acid esters, or metal esters of fatty acids. They lower the melt viscosity, internal friction, and promote fusion. When considering DDD, its structure closely resembles fatty acids. Indeed, the MFI results provide supportive evidence that DDD was responsible for a decrease in the PP melt viscosity by functioning as an internal lubricant. As a result of the improvement in this rheological property, the clay dispersibility in PP matrix was expectedly enhanced. In this study, an indirect, quantitative method was adopted to assess the uniformity of clay dispersion in PP matrix as follows: six samples of approx. 5 g composite compound each were randomly drawn from a composite resin and combusted at 1000°C to obtain the actual percent clay content. When compared among representative samples, the percent clay contents did not significantly differ (Fig. 7). Given the regularity of percent clay contents, we feel it is reasonable to imply that the dispersion of clay particles in the PP matrix is quite uniform.

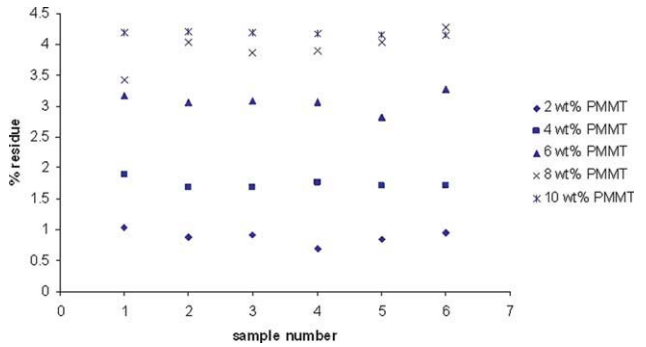

Figure 7 The percent clay contents of PP/PMMT nanocomposite fibers. [Color figure can be viewed in the online issue, which is available at www.interscience.wiley.com.]

X-ray analysis

X-ray patterns of the neat PP fibers and infused PMMT/PP fibers are shown in Figure 8. In all cases, α and β crystallinity forms show up strongly at $2\theta = 14$ and 16°, respectively, in the XRD diffractograms. For the neat PP fibers [Fig. 8(a)], the intensity of the peak associated with α crystallinity is relatively higher than that of β crystallinity, reflecting its higher content. In contrast, the intensity of α crystalline form tends to decrease in PMMT/PP composite fibers in association with an increase in the intensity of the β crystalline form. This indicates that the infusion of PMMT particles, with the assistance of a low speed take up is able to enhance the crystallization of the isotactic PP fiber. Typically, a higher content of the β -form crystallinity is desirable as it governs the balance between stiffness and flexibility of PP fibers. The degree of crystallinity, as derived from the XRD analysis, was not related to the percent clay loading, implying that the PP-clay interaction plays a dominant role in the crystallization process instead of the quantity as the nature of a nucleating agent has to be a very small particle to facilitate the optimum interfacial interaction. Despite its nanosized range, the size of these nanoparticles is still relatively large compared to inorganic salts, resulting in poorer nucleation efficiency. Therefore, an extra force, gained from the low take-up speed, was required to induce polymer orientation and crystallization.

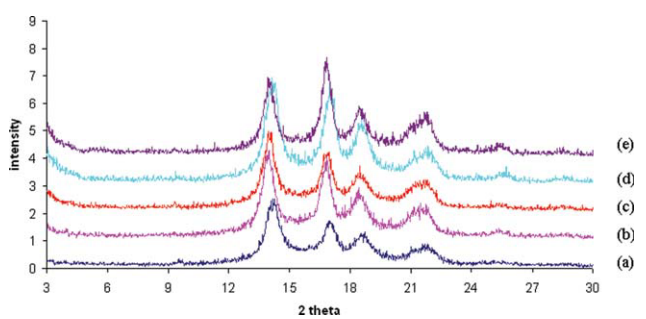

Figure 8 X-ray patterns of neat PP fibers and infused PP/PMMT nanocomposite fibers (a = neat fiber, b = 2 wt %, c = 4 wt %, d = 6 wt %, and e = 8 wt % PMMT). [Color figure can be viewed in the online issue, which is available at www.interscience.wiley.com.]

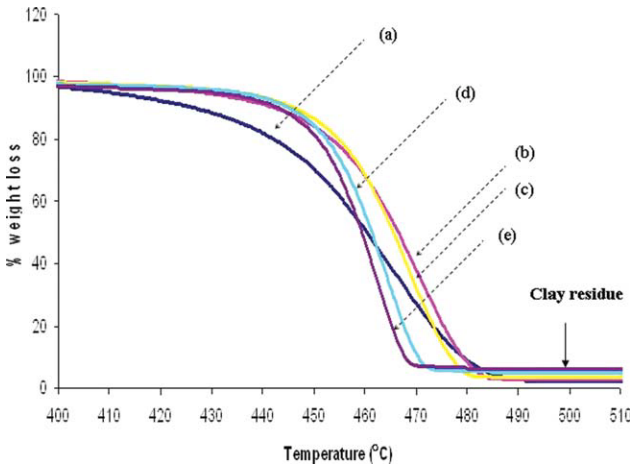

Figure 9 TGA thermograms of neat s (a) and PP/PMMT nanocomposite fibers (b = 2 wt %, c = 4 wt %, d = 6 wt % and e = 8 wt % PMMT). [Color figure can be viewed in the online issue, which is available at www.interscience.wiley.com.]

Thermogravimetric analyzer

The thermal stability of the fibers as well as particle–matrix interaction was evaluated by TGA analysis. Figure 9 shows representative TGA thermograms of the neat fiber [Fig. 9(a)] and PMMT filled fibers, whilst the onset temperatures of degradation are given in Table II. The neat fiber starts to decompose at 432.6°C, somewhat lower than that for the PMMT filled fibers, which began to decompose at 446.7°C (2 wt %), 448.8°C (4 wt %), 450.0°C (6 wt %), and 448.1°C (8 wt %). The reason for the additional increase in the onset temperature is that extra energy is required to break down the adhesion force at the polymer–PMMT particle interface. Therefore, the interfacial interaction plays an important role in the degradation of polymer nanocomposites. In the case of a good interfacial interaction, particles are capable of restricting the movement of a polymer chain, making the scission of polymer chains harder at

TABLE II
Thermal Properties of PP/PMMT Nanocomposites

PMMT loading (wt %)	T_c (°C)	H_f (J/g)	Degree of crystallinity	T_d (onset, °C)
0	109.22	78.68	47.21	432.60
2	109.90	74.32	45.74	446.90
4	109.87	69.74	44.05	448.80
6	109.89	63.80	41.39	450.00
8	109.58	64.22	42.83	448.10
10	110.56	61.02	41.86	447.80

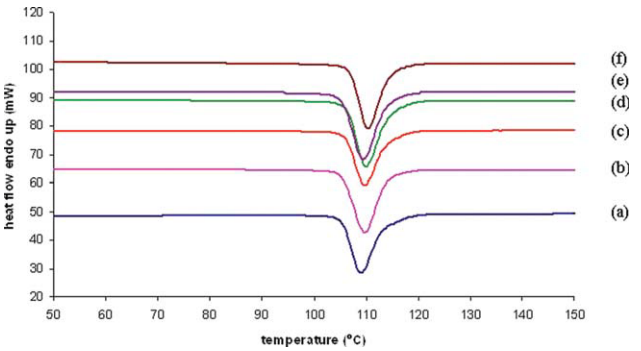

Figure 10 DSC curves of neat fibers (a) PP/PMMT nanocomposite fibers (b = 2 wt %, c = 4 wt %, d = 6 wt %, e = 8 wt %, and f = 10 wt % PMMT). [Color figure can be viewed in the online issue, which is available at www.interscience.wiley.com.]

lower temperatures. As a consequence, the degradation temperature of the nanocomposite shifts to a higher temperature. In addition, the presence of the interaction between clay layers and PP macromolecules was likely to inhibit the folding of PP macromolecule chains, resulting a decrease in PP crystallinity as presented in Table II. An increase in PMMT loading from 2 to 8 wt % does not result in an increase in the decomposition temperature since the higher PMMT loadings have a higher content of micron-sized particles. Micron-sized fillers are prone to exhibit poor adhesion to the polymer matrix due to their relatively small surface area. As a result, the effect of their presence on the degradation temperature is minuscule.

Differential scanning calorimetry analysis

The DSC curves of the composite fibers are shown in Figure 10, and their crystallization temperatures (T_c) and the percent crystallinity obtained from the DSC curves are given in Table II. The T_c value of virgin polypropylene fiber [Fig. 10(a)] appear at 109.22°C, whilst those for the composite fibers are not significantly different from the neat PP fibers, although the PP fibers containing 10 wt % PMMT exhibited a slightly higher T_c value than the others. This insignificant difference in the T_c values between the neat PP fibers and those with different ratios of PMMT included in the composite fibers may simply reflect a too small a sample weight (~3–4 mg) to be able to detect any slight but significant shift in the T_c value.

Fiber molecular orientation

Evaluation of the sonic modulus was used to determine the molecular orientation along the fiber axis. The transit time of the pulse sound was employed to calculate the sonic modulus according to eq. (1) (below), where the sonic modulus value (E, Young's modulus of elasticity (grams/denier)) is proportional to the molecular orientation in the fiber axis direction.

$$E = C^2K = C^2 11.3 = \text{sound velocity (km/sec)}; \quad (1)$$

Where C = distance (centimeters) $\times 10^{-5}$, Transit time (microseconds) $\times 10^{-6}$ and K = a constant conversion factor of 11.3.

The sonic modulus values (mean + 1 S.D.) of PP/PMMT nanocomposite fibers containing 0, 2, 4, 6, and 8 wt % PMMT were 32.36 + 4.08, 34.04 + 10.16, 43.88 + 11.12, 36.88 + 7.99, and 30.61 + 4.01, respectively. Thus, as the PMMT loading is increased from 2 to 6 wt %, the sonic modulus value increases gradually, indicating that an increase in PMMT content results in an increase in polymer orientation along fiber axis. However, this does not hold at 8 wt % where the sonic modulus falls to a lower value, less than even that for the neat PP fibers. Referring to the MFI measurements, a steady increase in the MFI of the nanocomposite was observed with increasing PMMT loadings. The results show that an increase in the melt flowability of the nanocomposite helps enhance polymer chain alignment along the fiber axis, as evidenced by the increased sonic modulus values. However, as mentioned above, above 6 wt % PMMT loading, the sonic modulus value decreases and it is likely that the density of the dispersed PMMT particles reached a level where the degree of polymer chain orientation was interfered with.

Mechanical properties

The mechanical properties of the composite fibers were measured with a universal testing machine (Instron 5583), in terms of the tensile strength and % elongation at break, according to ASTM D3822. 5 representative samples were employed for each PP/PMMT formulation. The tensile strength values of

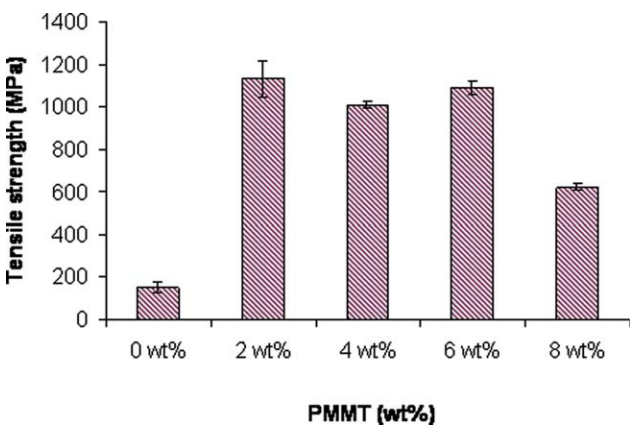

Figure 11 Tensile strength of PP/PMMT nanocomposite fibers compared with the neat PP fibers. [Color figure can be viewed in the online issue, which is available at www.interscience.wiley.com.]

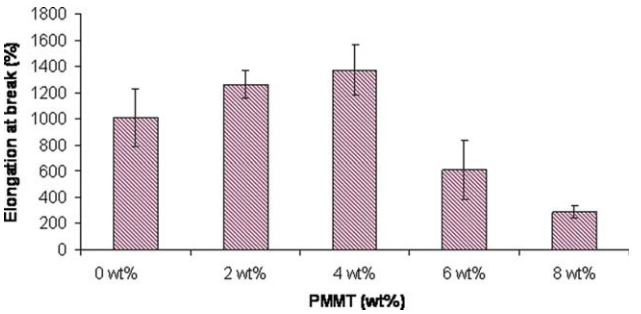

Figure 12 Percent elongation of PP/PMMT nanocomposite fibers compared with the neat PP fibers. [Color figure can be viewed in the online issue, which is available at www.interscience.wiley.com.]

composite fibers containing 0, 2, 4, 6, and 8 wt % PMMT were about 150, 1132, 1012, 1093, and 619 MPa, respectively (Fig. 11). The % elongation values (Fig. 12) also show a similar trend of increasing with increasing levels of PMMT from 2 to 6 wt % and then falling at 8 wt %, with values of 1011, 1263, 1373, 612, and 293 for 0, 2, 4, 6, and 8 wt % PMMT, respectively. Thus, the effect of PMMT addition could significantly enhance as well as severely impair the mechanical properties depending on the wt % addition. The addition of PMMT in the range of 2–6 wt % significantly improved the mechanical properties of the composite fiber, indicating that the incorporation of the PMMT filler into PP fiber leads to an improvement in the tensile strength due to a reinforcement effect derived from the unique characteristic of its large aspect ratio. However, a higher PMMT content, such as 8 wt %, brought about an adverse effect on the mechanical properties, as evidenced by a significant decrease in the tensile strength, reflecting that the particle size and distribution are the crucial factors affecting the mechanical properties of typical nanocomposite materials. In this case, at a low PMMT content, monmorillonite exists in an exfoliation state that maximizes the adhesion of PMMT particles to the PP matrix due to its large surface area. Furthermore, due to its good compatibility with the PP matrix, the fine particles are easily dispersed, resulting in a good particle distribution. On the other hand, an excess PMMT content was a likely to cause phase separation and a poor particle distribution leading to poor mechanical properties, as observed by the sharp decrease in the tensile strength at 8 wt % PMMT. Therefore, the amount of PMMT addition is an important factor for the preparation of nanocomposite materials.

CONCLUSION

This study demonstrated that the *in situ* conversion of intercalated dodecylamine to dodecylamino dimethylene diphosphonic acid resulted in changes in the particle size, dimensions, and morphology of montmorillonite clay. It is proposed that the dodecylamino dimethylene diphosphonic acid caused the expansion of the clay gallery and prevented the restacking of separated clay sheets to the original form. A formation of large platelets with a relatively large interlayer spacing compared to the organoclay was obtained. TEM analysis suggests an extremely fine clay was accomplished by the formation of the dodecylamino dimethylene diphosphonic acid guest molecule, which we propose could separate the clay platelet stacks by creating a powerful repulsion force between the dodecylamino dimethylene diphosphonic acid group and negative charge clay.

PMMT loading into PP fibers led to a nucleation effect on the polymer crystallization process, resulting in an increase in β-form crystallinity. The polymer chain orientation in the fiber axis direction was increased in the 2–6 wt % PMMT filled PP fibers, resulting from an increase in melt flowability of the composite resin. Finally, the thermal stability of PP fibers could be improved when filled with PMMT at up to 6 wt % in comparison with neat PP fiber.

The authors thank Dr. Robert Butcher (PCU Unit, Faculty of Science, Chulalongkorn University) for English corrections.

References

1. Usuki, A.; Kojima, Y.; Kawasumi, M.; Okada, A.; Fukushima, Y.; Kurauchi, T.; Kamigaito, O. J Mater Res 1993, 8, 1179.
2. Burnside, S. D.; Giannelis, E. P. Chem Mater 1995, 7, 1597.
3. Thellen, C.; Orroth, C.; Froio, D.; Ziegler, D.; Lucciarini, J.; Farrell, R.; D'Souza, N.; Ratto, J. Polymer 2005, 46, 11716.
4. Venugopal, B. R.; Rajamathi, M. Appl Clay Sci 2008, 41, 143.
5. Limpanart, S.; Khunthon, S.; Taepaiboon, P.; Supaphol, P.; Srikhirin, P.; Udomkichdecha, W.; Boontongkong, Y. Mater Lett 2005, 59, 2292.
6. Osman, A.; Rupp, J. E. P.; Suter, U. W. Polymer 2005, 46, 8202.
7. Zhong, Y.; Zhu, Z. Y.; Wang, S. Q. Polymer 2005, 46, 3006.
8. Vazquez, A.; Lopez, M.; Kortaberria, G.; Martin, L.; Mondragon, I. Appl Clay Sci 2008, 41, 24.
9. Wang, Z. B.; Wang, X.; Li, G. C.; Zhang, Z. K. Appl Clay Sci 2008, 42, 146.
10. Velasco, J. J.; De, S.; Martinez, A. J Appl Polym Sci 1996, 61, 125.
11. Qiu, W.; Mai, K.; Zeng, H. J Appl Polym Sci 2000, 77, 2974.
12. Amash, A.; Zugenmaier, P. Polymer 2000, 41, 1589.
13. Esfandiari, A. Fiber Polym 2008, 9, 48.
14. Sui, G.; Fuqua, M. A.; Ulven, C. A.; Zhong, W. A. Bioresour Technol 2009, 2, 1246.
15. Bhattacharyya, A. R.; Sreekumar, T. V.; Liu, T.; Kumar, S.; Ericson, L. M.; Robert, H. H.; Hauge, H.; Smalley, R. E. Polymer 2003, 44, 2373.
16. Chatterjee, A.; Deopura, B. L. Fiber Polym 2003, 4, 102.
17. Liu, X.; Wu, Q. Polymer 2001, 42, 10013.
18. Gao, F. Mater Today 2004, 7, 50.
19. Punyacharoennon, P.; Charuchinda, S.; Srikulkit, K. J Appl Polym Sci 2008, 110, 3336.
20. Grutzner, T.; Hasse, H.; Lang, N.; Siegert, M.; Strofer, E. Chem Eng Sci 2007, 62, 5613.